High-resolution Structure of the Phosphorylated Form of the Histidine-containing Phosphocarrier Protein HPr from Escherichia coli Determined by Restrained Molecular Dynamics from N...

ARTICLE *in* JOURNAL OF MOLECULAR BIOLOGY · MARCH 1995

Impact Factor: 4.33 · DOI: 10.1006/jmbi.1994.0075 · Source: OAI

4 AUTHORS:

Nico A J Van Nuland
Vrije Universiteit Brussel
97 PUBLICATIONS **2,575** CITATIONS
SEE PROFILE

Rolf Boelens
Utrecht University
360 PUBLICATIONS **13,840** CITATIONS
SEE PROFILE

Ruud M. Scheek
University of Groningen
104 PUBLICATIONS **3,785** CITATIONS
SEE PROFILE

George Robillard
University of Groningen
152 PUBLICATIONS **3,937** CITATIONS
SEE PROFILE

J. Mol. Biol. (1995) **246**, 180–193

JMB

High-resolution Structure of the Phosphorylated Form of the Histidine-containing Phosphocarrier Protein HPr from *Escherichia coli* Determined by Restrained Molecular Dynamics from NMR-NOE Data

Nico A. J. van Nuland[1], Rolf Boelens[2], Ruud M. Scheek[1]* and George T. Robillard[1]

[1]*Groningen Biomolecular Sciences and Biotechnology Institute and the Department of Biochemistry and Biophysical Chemistry University of Groningen Nijenborgh 4, 9747 AG Groningen, The Netherlands*

[2]*Bijvoet Centre for Biomolecular Research University of Utrecht Transitorium 3, Padualaan 8 Utrecht, The Netherlands*

**Corresponding author*

The solution structure of the phosphorylated form of the histidine-containing phosphocarrier protein, HPr, from *Escherichia coli* has been determined by NMR in combination with restrained molecular dynamics simulations. The structure of phospho-HPr (*P*-HPr) results from a molecular dynamics simulation in water, using time-dependent distance restraints to attain agreement with the measured NOEs. Experimental restraints were identified from both three-dimensional ^{1}H-^{1}H-^{15}N HSQC-NOESY and two-dimensional ^{1}H-^{1}H NOESY spectra, and compared with those of the unphosphorylated form. Structural changes upon phosphorylation of HPr are limited to the active site, as evidenced by changes in chemical shifts, in $^{3}J_{NHH\alpha}$-coupling constants and NOE patterns. Chemical shift changes were obtained mainly for protons that were positioned close to the phosphoryl group attached to the His15 imidazole ring. Differences could be detected in the intensity of the NOEs involving the side-chain protons of His15 and Pro18, resulting from a change in the relative position of the two rings. In addition, a small change could be detected in the three-bond *J*-coupling between the amide proton and the H^{α} proton of Thr16 and Arg17 upon phosphorylation, in agreement with the changes of the ϕ torsion angle of these two residues obtained from time-averaged restrained molecular dynamics simulations in water. The proposed role of the torsion-angle strain at residue 16 in the mechanism of *Streptococcus faecalis* HPr is not supported by these results. In contrast, phosphorylation seems to introduce torsion angle strain at residue His15. This strain could facilitate the transfer of the phosphoryl group to the A-domain at enzyme II. The phospho-histidine is not stabilised by hydrogen bonds to the side-chain group of Arg17; instead stable hydrogen bonds are formed between the phosphate group and the backbone amide protons of Thr16 and Arg17, which show the largest changes in chemical shift upon phosphorylation, and a hydrogen bond involving the side-chain O^{γ} proton of Thr16.

HPr accepts the phosphoryl group from enzyme I and donates it subsequently to the A domain of various enzyme II species. The binding site for EI on HPr resembles that of the A domain of the mannitol-specific enzyme II, as can be concluded from the changes on the amide proton and nitrogen chemical shifts observed *via* heteromolecular single-quantum coherence spectroscopy.

Keywords: phosphorylation; *P*-HPr; nuclear magnetic resonance; molecular dynamics; EI binding-site

Abbreviations used: PEP, phospho*enol*pyruvate; EI, enzyme I; PTS, PEP-dependent phosphotransferase system; HPr, histidine-containing phosphocarrier protein; *P*-HPr, phospho-HPr; MD, molecular dynamics; NOE, nuclear Overhauser effect; TOCSY, total correlation spectroscopy; NOESY, NOE spectroscopy; HMQC, heteronuclear multiple-quantum coherence spectroscopy; HSQC, heteronuclear single-quantum coherence spectroscopy; ^{15}N-HSQC-NOESY, 3D ^{1}H-^{15}N single-quantum coherence ^{1}H-^{1}H NOE spectroscopy; 2D, 3D, 4D, two-, three, four-dimensional; TPPI, time-proportional phase incrementation; p.p.m., parts per million; IIA^{mtl}, the A domain of the mannitol enzyme II; IIA^{glc}, the A domain of the glucose enzyme II; r.m.s., root-mean-square; r.m.s.d., r.m.s. difference.

0022–2836/95/060180–14 $08.00/0

Introduction

For the last three years much effort has been spent on resolving the structural details of the active site of HPr in an effort to explain its function in the transfer of a phosphoryl group from phospho*enol*pyruvate (PEP) *via* enzyme I (EI) to enzyme II (EII) in the phospho*enol*pyruvate-dependent phosphotransferase system (PTS; see for reviews, Postma *et al*., 1993; Lolkema & Robillard, 1993; Reizer *et al*., 1993). A prerequisite for a complete understanding of the reaction mechanism is a high-resolution structure of phospho-HPr (*P*-HPr), which has not yet been forthcoming. Phosphorylation of HPr occurs at the $N^{\delta 1}$ position of the His15 imidazole ring (Weigel *et al*., 1982; Waygood *et al*., 1985; Van Dijk *et al*., 1990).

Jia *et al*. (1993*a*, 1994) compared X-ray structures of HPr with and without sulphate bound near the active site. On the assumption that the sulphate was equivalent to a phosphate analogue, they proposed that the differences in structures represented the changes that occur during a phosphorylation/dephosphorylation cycle. They suggested that the imidazole ring of the active site residue 15 and the Arg17 side-chain cycle between different relative positions according to the phosphorylation state of the protein. The unfavourable ϕ, ψ torsion angles of residue 16 in the *Streptococcus faecalis* HPr (Jia *et al*., 1993*a*, 1994) structure, which lacks sulphate, were interpreted as strain in the molecule. Upon phosphorylation this would be released, accounting for the absence of strain in the *Bacillus subtilis* structure (Herzberg *et al*., 1992), which contains sulphate. The X-ray structure of *Escherichia coli* HPr (Jia *et al*., 1993*b*) also contains a sulphate ion in the active centre but was found to possess an intermediate conformation, half-way between the proposed phosphorylated and unphosphorylated forms. In contrast to the X-ray structure, our high-resolution NMR structure of unphosphorylated *E. coli* HPr (Van Nuland *et al*., 1994), shows no unfavourable torsion angles. Molecular dynamics (MD) simulations showed that the Arg17 side-chain could cover a wide range of positions relative to the His15 imidazole ring. On the basis of these observations we concluded that the different X-ray structure positions of the Arg17 and His15 side-chains were caused by the different crystal packings and/or the presence of a sulphate ion. In contrast to the proposal of Jia *et al*. (1993*a*), we have evidence that the His15 φ, ψ torsion angles of HPr become strained upon phosphorylation.

Here we present the structure of *P*-HPr resulting from MD simulations in water, using time-dependent distance restraints to attain agreement with the measured *P*-HPr NOEs. The high-resolution structure of the unphosphorylated form of *E. coli* HPr has already been obtained by the combined use of NMR and MD simulations based on 1520 experimental restraints (Van Nuland *et al*., 1994). By comparing the unphosphorylated and phosphorylated forms of *E. coli* HPr, the structural changes that occur at the active site, as evidenced by changes in chemical shifts, in $^3J_{NHH\alpha}$-coupling constants and NOE patterns, can be clearly defined.

Results

Assignment of backbone and side-chain protons in *P*-HPr and identification of NOE differences

The complete assignments of all HPr backbone and side-chain protons were reported earlier (Van Nuland *et al*., 1992*a*,*b*). ^{1}H traces in the 2D TOCSY, 2D NOESY and 3D HSQC-NOESY spectra of HPr were compared with those of *P*-HPr, and sequential contacts in the NOESY spectra were checked for both forms of the protein. Figure 1 shows an overlay of two ^{15}N-HSQC spectra of ^{15}N-enriched HPr, recorded before and after phosphorylation of His15. The chemical shifts of the ^{1}H-^{15}N moieties of the active-site residues His15, Thr16 and Arg17 are most strongly affected. Table 1 summarises the frequencies of all protons and nitrogens that shift more than 0.03 p.p.m. (^{1}H) or 0.20 p.p.m. (^{15}N) upon phosphorylation. In general, only protons in close proximity to the active site are affected.

In the NOESY spectra, differences in NOE patterns and intensities could be observed between HPr and *P*-HPr only for protons of active-site residues, most notably His15 and Pro18, which also indicates that structural rearrangements occur only in the active site. We used ^{15}N-HSQC spectroscopy to check the phosphorylation state of HPr before and after the more time-consuming 2D and 3D NOESY experiments. During about 20 hours after the addition of EI, hydrolysis of *P*-HPr causes the depletion of the excess of PEP. After this time the HPr cross-peaks reappear in HSQC spectra and gain intensity at the expense of those of *P*-HPr. Figure 2 illustrates some of the differences in NOEs involving backbone amide protons at the active site. Figure 2A shows four 2D slices taken from the 3D HSQC-NOESY spectrum of HPr at the ^{1}H frequencies corresponding to the backbone amide protons of residues 15, 16, 17 and 19. Figure 2B shows the corresponding slices for *P*-HPr. Table 2 summarises the observed NOE differences. A total of 1519 and 1508 distance restraints was extracted from the NOESY spectra of HPr and *P*-HPr, respectively. For HPr and *P*-HPr 369 of these restraints were intraresidual $(i, i + j | j = 0)$, 413 and 410 were sequential $(i, i + j | j = 1)$, 288 and 278 were medium-range $(i, i + j | 2 \leqslant j \leqslant 4)$, and 449 and 451 were long-range $(i, i + j | j > 4)$, respectively.

The backbone amide proton of His15 in *P*-HPr has a relatively low intensity, which we attribute to the exchange between protonated and deprotonated states of the phosphorylated His ring at pH 7.5, close to its pK_a of 7.8 (Dooijewaard *et al*., 1979). In our earlier work on unphosphorylated HPr the same phenomenon was observed at pH 6.5, close to the pK_a of the unphosphorylated His ring. The rationale for

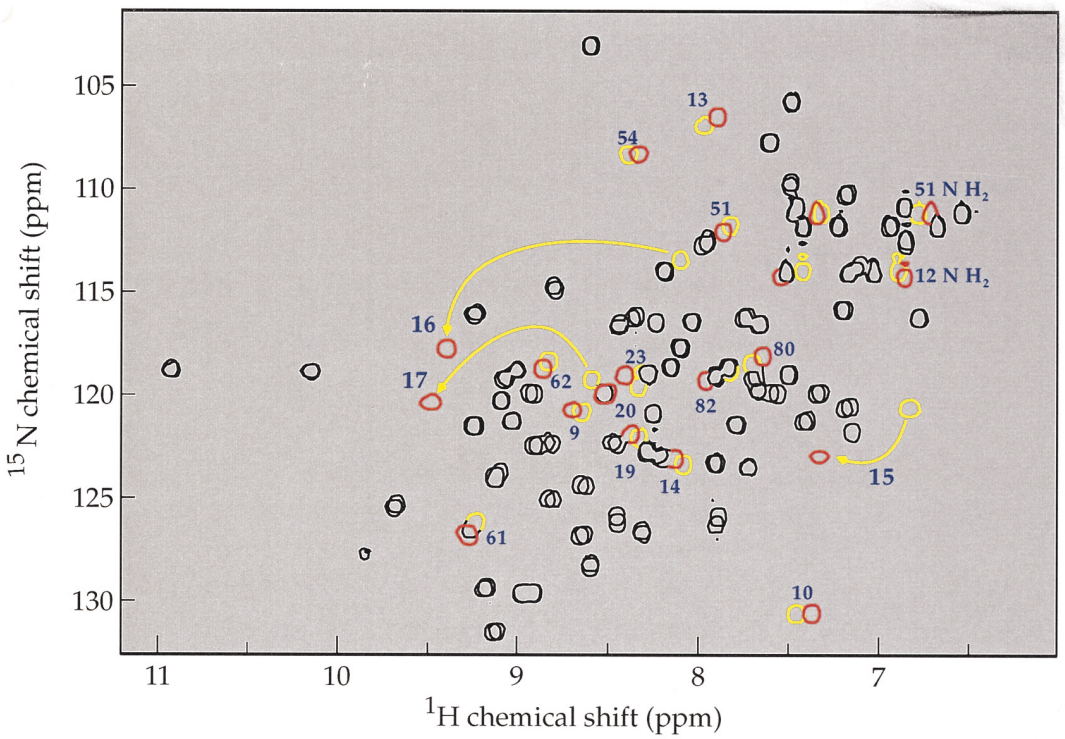

Figure 1. An overlay of the 500 MHz ^{15}N-HSQC spectra of ^{15}N-enriched HPr and P-HPr. Cross-peaks that do not shift substantially upon phosphorylation are represented by black contours for both forms of the protein. Cross-peaks that shift upon phosphorylation are represented by yellow contours for HPr and red contours for *P*-HPr. Spectra were recorded at 20°C in 50 mM KP_i, 90 mM phospho*enol*pyruvate (PEP), 1 mM $MgCl_2$ (pH 7.5). HPr was phosphorylated by adding 50 µl of a 0.2 mM EI solution to the NMR sample. Cross-peaks in these spectra arise from protons that have a 1-bond *J*-coupling to ^{15}N nuclei. Cross-peaks that shift more than 25 Hz upon phosphorylation are labelled with the residue number to which they have been assigned. In addition, 2 side-chain NH_2 groups (Asn12 and Gln51) are indicated.

the low intensity is supported in our present study where spectra of HPr were collected at pH 7.5 for a direct comparison with those of *P*-HPr at the same pH. pH 7.5 is well removed from the pK_a of His15 in HPr and at this pH the His15 amide proton of HPr shows a normal intensity.

In our earlier work on the structure of HPr at pH 6.5 and 30°C (Van Nuland *et al*., 1994), we observed several NOEs to a hydroxyl proton, which we assigned to Ser31. This proton was also identified in the NMR spectra of *Staphylococcus aureus* HPr (Kalbitzer & Hengstenberg, 1993). Hammen *et al*. (1991) observed an additional hydroxyl proton with a chemical shift of 5.31 p.p.m. in their spectra recorded on *E. coli* HPr under the same experimental conditions. On the basis of the observation of NOEs of this proton to the C^{α} and/or C^{β} (their chemical shifts coincide) and $C^{\gamma}H_3$ protons of Thr59, they assigned this proton to Thr59 $O^{\gamma}H$. We did not observe this proton in the NOE spectra at pH 6.5 and 30°C. In our present work we recorded all spectra at pH 7.5 and 20°C, and we identified a proton with a chemical shift of 5.25 p.p.m. Low intensity NOEs could be observed from this proton to the Ser37 C^{β} protons, Thr59 $C^{\gamma}H_3$ protons and to two other side-chain protons, most probably belonging to the two $C^{\delta}H_3$ groups of Leu55. No NOEs could be observed to either the C^{α}/C^{β} protons of Thr59 or to the H^{α} of Ser37. It remains uncertain whether this resonance belongs to the Ser37 $O^{\gamma}H$ or Thr59 $O^{\gamma}H$. This proton could not be detected in the spectra of *P*-HPr.

The three-bond *J*-coupling experiments: comparison of the HMQC spectra

The NH-$C^{\alpha}H$ coupling constants were measured for all residues in HPr and *P*-HPr, except for Met1, Pro11, His15, Pro18 and Asn38. Figure 3 shows the $\omega 1$ (^{15}N) traces at the ^{1}H frequencies of the amide protons of Thr16 (A) and Arg17 (B), taken from the HMQC spectra of HPr and *P*-HPr. In these traces the three-bond *J* coupling between amide and H^{α} protons causes the formation of ^{15}N doublets, which, if unresolved, simply shows up as an extra contribution to the observed linewidth. The increase in the coupling constants of Thr16 and Arg17 upon phosphorylation is apparent from additional broadening of the ^{15}N resonances of these residues, and is in agreement with the change in the φ dihedral angles observed for these residues in the MD simulations, which will be described below. Small changes around residue 62 are accompanied by chemical shift changes in the nearby backbone ^{15}N atoms of Val35, Val61 and Thr62. The observed coupling constants for all other residues correspond well with the secondary structure elements identified in HPr (Van Nuland *et al*., 1992*b*). The lack of substantial changes in these coupling constants upon

Table 1

Backbone and side-chain ^{1}H and ^{15}N chemical shifts for *E. coli P*-HPr at pH 7.5 and 20°C, 50 mM potassium phosphate

Atom†	P-HPr chemical shift‡ (p.p.m.)	P-HPr–HPr chemical shift§ (p.p.m.)	Atom	P-HPr chemical shift‡ (p.p.m.)	P-HPr–HPr chemical shift§ (p.p.m.)
8 Ile $H^{\gamma 12}$	1.136	0.056	19 Ala H^{α}	3.840	0.050
9 Thr NH	8.744	0.056	19 Ala H^{β}	1.226	0.056
10 Ala NH	7.396	– 0.092	20 Ala N	118.99	0.28
12 Asn $N^{\delta 2}$	113.44	0.27	20 Ala NH	8.533	0.164
12 Asn $H^{\delta 21}$	7.579	0.116	23 Val NH	8.452	0.097
12 Asn $H^{\delta 22}$	6.884	– 0.049	26 Ala NH	8.881	0.035
13 Gly N	108.81	– 0.49	38 Asn NH	9.800	– 0.093
13 Gly NH	7.923	– 0.087	35 Val N‖	125.98	0.30
14 Leu NH	8.172	0.047	48 Phe N	115.32	– 0.24
14 Leu H^{α}	4.496	0.032	48 Phe NH	8.370	– 0.032
14 Leu $H^{\beta 2}$	1.011	0.063	50 Leu NH	8.659	– 0.034
14 Leu H^{γ}	1.303	0.114	51 Gln N	111.29	0.33
14 Leu $H^{\delta 1}$	0.691	0.056	51 Gln NH	7.902	0.039
14 Leu $H^{\delta 2}$	0.505	0.056	51 Gln $H^{\epsilon 22}$	6.755	– 0.063
15 His N	122.07	2.24	54 Gly NH	8.376	– 0.054
15 His NH	7.312	0.452	55 Leu N	124.95	– 0.37
15 His $H^{\beta 1}$	3.982	0.503	56 Thr N	109.64	0.20
15 His $H^{\beta 2}$	3.472	0.332	56 Thr H^{α}	4.228	0.035
15 His $H^{\delta 2}$	7.105	– 0.123	57 Gln NH	8.855	– 0.031
15 His $H^{\epsilon 1}$	8.214	0.390	61 Val N‖	125.78	0.55
16 Thr N	116.95	4.19	61 Val NH	9.308	0.033
16 Thr NH	9.454	1.316	61 Val H^{α}	4.898	– 0.042
16 Thr H^{β}	4.339	0.137	62 Thr N	118.00	0.42
17 Arg N	119.56	1.16	62 Thr NH	8.904	0.030
17 Arg NH	9.548	0.919	80 Leu N	117.34	– 0.37
17 Arg H^{α}	4.223	– 0.082	80 Leu NH	7.682	– 0.063
17 Arg $H^{\beta 1}$	1.951	– 0.032	80 Leu $H^{\beta 2}$	1.685	0.041
17 Arg $H^{\beta 2}$	1.863	– 0.044	80 Leu H^{γ}	1.460	– 0.030
17 Arg $H^{\gamma 1}$	1.716	– 0.062	81 Met H^{α}	4.040	0.030
17 Arg $H^{\gamma 2}$	1.716	0.114	81 Met $H^{\beta 2}$	2.032	– 0.031
18 Pro $H^{\beta 1}$	2.233	0.080	82 Ala N	118.42	0.36
18 Pro $H^{\beta 2}$	1.975	0.283	82 Ala NH	8.019	0.153
18 Pro $H^{\gamma 1}$	1.744	0.055	83 Glu $H^{\gamma 1}$	2.458	0.033
18 Pro $H^{\gamma 2}$	1.744	0.174	84 Leu $H^{\beta 2}$	1.489	0.061
18 Pro $H^{\delta 1}$	3.230	0.155	84 Leu H^{γ}	1.489	0.061
19 Ala NH	8.429	0.058	85 Glu N	125.41	0.35

Values are given only for protons / nitrogens which differ more than 0.03 p.p.m. (^{1}H) and 0.20 p.p.m. (^{15}N) from HPr.

† Non-equivalent methylene protons or methyl groups are arbitrarily labelled 1 and 2 for the low-field and high-field resonances, respectively.

‡ ^{1}H chemical shifts are expressed relative to trimethylsilylpropanesulfonic acid, ^{15}N shifts relative to liquid NH_3 (Live *et al*., 1984).

§ The shift is defined as the difference between the *P*-HPr and the HPr frequencies.

‖ The ^{15}N-^{1}H cross-peaks for Val35 and Val61 overlap in *P*-HPr.

phosphorylation indicates that no large structural changes in the backbone are to be expected.

Structure calculations: restrained MD and free MD simulations on HPr and *P*-HPr

We modelled *P*-HPr as follows. Starting from unphosphorylated HPr (Van Nuland *et al*., 1994), we introduced the phosphoryl group at the $N^{\delta 1}$ position of His15 and performed a 200 picosecond restrained MD simulation in water in a time-dependent manner using the distance restraints derived from the measured NOEs of *P*-HPr. The resulting set of *P*-HPr conformations stays close to the set found for the unphosphorylated form, with a root-mean-square (r.m.s.) positional difference calculated for the backbone atoms of residues 2 to 84 of only 0.081 nm between the average structures. Figure 4A compares the r.m.s. C^{α} positional differences for sets of 20 snapshots taken from time-averaged MD trajectories on HPr and *P*-HPr. The fluctuations along the amino acid sequence are comparable for both forms of the protein. Figure 4B shows that the main structural differences between the two averaged structures are concentrated around the active centre. Large r.m.s. C^{α} positional differences between the two average structures are observed for residues close to the active site. Remaining NOE violations, atomic r.m.s.d. values and other structural statistics are collected in Table 3. The small but significant structural rearrangements that occur at the active site are shown in Figure 5A. Upon phosphorylation, the Arg17 side-chain occupies a different ensemble of positions. The *P*-His15 imidazole ring rotates over a rather small distance away from the position perpendicular to the Pro18 ring. This is accompanied

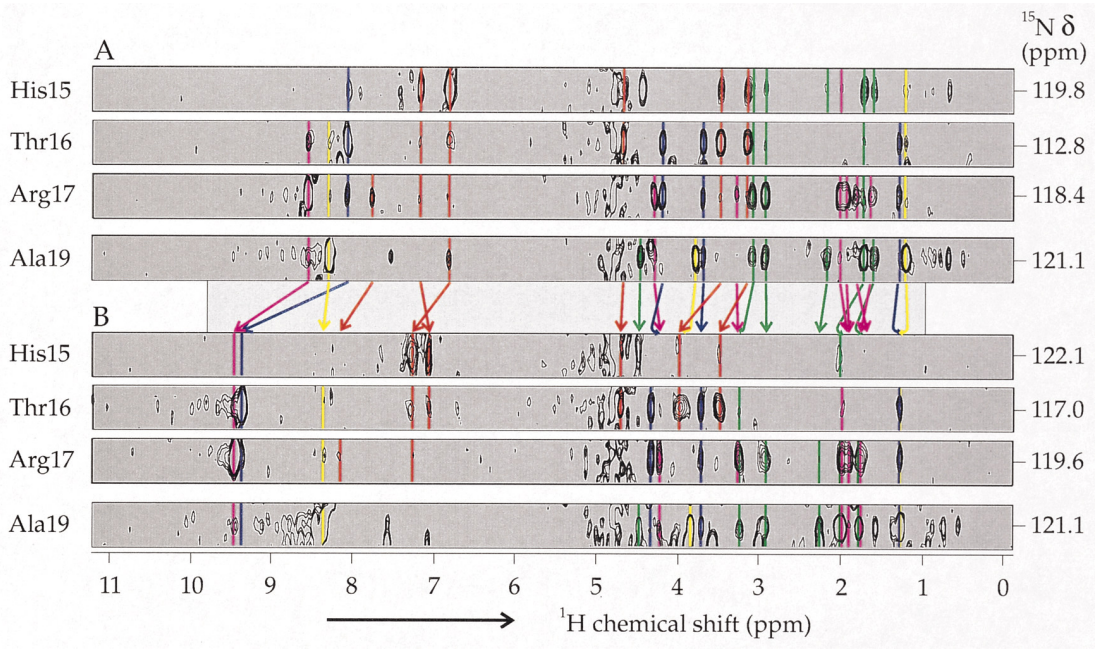

Figure 2. Selected contour plots of slices taken from the 2 3D HSQC-NOESY spectra of HPr and *P*-HPr at 20°C (pH 7.5). Each slice shows the ^{1}H ($\omega 3$) frequency domain and a narrow band around the ^{15}N ($\omega 2$) chemical shift (δ) of the corresponding ^{1}H-^{15}N spin pair of residues 15, 16, 17 and 19. Cross-peaks arising from protons of His15 are coloured in red, from Thr16 in blue, from Arg17 in purple, from Pro18 in green, and from Ala19 in yellow. Arrows between A and B correspond to the changes in chemical shift upon phosphorylation. A, HPr; B, *P*-HPr.

by a change in the position of the main-chain atoms around *P*-His15 and results in the introduction of unfavourable φ, ψ dihedral angles at *P*-His15.

The position of the *P*-His15 is stabilised by an extensive hydrogen-bonding network (Figure 5B). The acceptor for the H-bond with the amide proton of Ala19 changes from the carbonyl oxygen of His15 in HPr to that of Leu14 in *P*-HPr. The H-bond between the amide proton of Leu14 and the carbonyl oxygen of Leu55, which is observed in all unphosphorylated HPr structures, is destabilised somewhat (from 70% to 55%, see Figure 6) upon phosphorylation. A stable H-bond is formed between the His15 amide proton and the carbonyl oxygen of Leu55. In addition, a stable H-bond is formed between the side-chain NH_2 group of Gln51 and the backbone carbonyl group of Thr16. The proximity of the Gln51 side-chain NH_2 group to the active site is evident from NOE between the Gln51 $H^{\epsilon}22$ and Thr16 H^{β} protons and explains the chemical shift changes of the Gln51 side-chain ^{1}H and ^{15}N resonances upon phosphorylation (Figure 1). The phosphoryl group is not stabilised by H-bonds to the side-chain of Arg17, as suggested by other investigators (Jia *et al*., 1993*a*; Herzberg *et al*., 1992). Instead, stable H-bonds are formed between the

Table 2

NOEs involving the active site residues 15, 16, 17, 18 and 19

Proton (donor)	Proton (acceptor)	HPr	P-HPr	Proton (donor)	Proton (acceptor)	HPr	P-HPr
15 His NH	14 Leu H^{γ}	w	–	15 His $H^{\epsilon 1}$	18 Pro $H^{\gamma 1}$	w	–
	14 Leu $H^{\beta 1}$	w	–		18 Pro $H^{\gamma 2}$	w	–
	14 Leu $H^{\beta 2}$	w	–		18 Pro $H^{\delta 2}$	m	vw
	14 Leu $H^{\delta 1}$	m	–	16 Thr NH	15 His $H^{\delta 2}$	vw	w
	15 His $H^{\beta 1}$	m	w		18 Pro $H^{\beta 2}$	vw	–
	15 His $H^{\delta 2}$	m	s		18 Pro $H^{\delta 2}$	vw	–
	16 Thr NH	w	–		19 Ala NH	vw	–
	18 Pro $H^{\beta 1}$	vw	–	16 Thr H^{β}	51 Gln $H^{\epsilon 22}$	–	vw
	18 Pro $H^{\beta 2}$	s	m	17 Arg NH	15 His $H^{\beta 1}$	vw	–
	18 Pro H^{γ}	m	–		15 His $H^{\beta 2}$	vw	–
	18 Pro $H^{\delta 1}$	w	–		15 His $H^{\delta 2}$	vw	–
	18 Pro $H^{\delta 2}$	w	–		15 His $H^{\epsilon 1}$	m	vw
	19 Ala H^{β}	w			17 Arg H^{γ}	w	m
15 His $H^{\delta 2}$	14 Leu H^{α}	w	m		18 Pro $H^{\delta 2}$	s	m
	18 Pro $H^{\delta 1}$	vw	–	17 Arg H^{α}	21 Gln NH	vw	–
				19 Ala NH	15 His NH	w	–

Only NOEs that show difference in intensity in the *P*-HPr NOE spectra related to the HPr spectra are given: not present (–); very weak NOE (vw); weak NOE (w); medium NOE (m); and strong NOE (s).

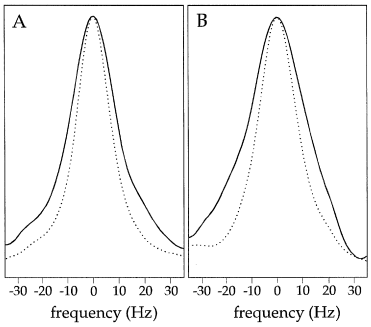

Figure 3. ω1-(^{15}N-) traces at the ^{1}H chemical shifts of the amide protons of Thr16 (A) and Arg17 (B) taken from HMQC spectra of HPr (dotted lines) and *P*-HPr (continuous lines), recorded at 600 MHz. In these traces the 3-bond *J* coupling between amide and H^{α} protons causes the formation of ^{15}N doublets, which, if unresolved, simply shows up as an extra contribution to the observed linewidth.

phosphate oxygens and the backbone amide protons of Thr16 and Arg17, in complete agreement with the large chemical-shift differences observed for these protons upon phosphorylation. An H-bond is also present between the phosphate oxygen and the side-chain O^{γ} proton of Thr16. These H-bonds were proposed by Herzberg *et al.* (1992) on the basis of modelling studies. Stabilisation of a phosphate by H-bonding to the main-chain amide protons at the N terminus of an α-helix, as we find for *P*-HPr, has been found in several enzymes (Johnson & Barford, 1993). This arrangement is favoured by the helix macrodipole, which arises from the alignment of the peptide dipoles parallel to the helix axis (Hol *et al*., 1978). Figure 6 shows the H-bond stability of all backbone amide protons, calculated from the two time-averaged restrained MD trajectories on HPr and *P*-HPr. The H-bond network is similar for HPr and *P*-HPr, except for H-bonds involving residues in the active centre and residues in the small helix, ranging from Leu47 to Thr52. The helix is less well defined in *P*-HPr. The region where these changes occur are involved in binding to EI and IIA^{mtl}; the amide protons of these residues show changes in chemical shift upon phosphorylation. The differences in the H-bond stability in the region ranging from Val60 to Ile63 upon phosphorylation may explain the chemical shift changes in this region (Table 3), as well as small changes in the three-bond $J_{HNH\alpha}$ coupling constants around residue 62, as measured in the HMQC spectra (data not shown).

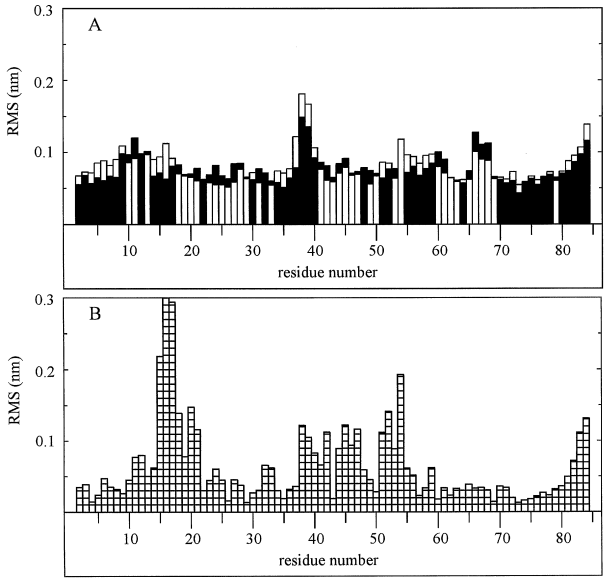

Figure 4. The r.m.s. C^{α} positional differences along the amino acid sequence. A, The r.m.s. C^{α} positional differences for 20 snapshots taken from time-averaged MD trajectories of HPr (open bars) and of *P*-HPr (filled bars). B, The r.m.s. C^{α} positional differences between the 2 average structures of HPr and *P*-HPr.

Figure 7 visualises the changes that occur in the average φ, ψ torsion angles for residues 15 (filled squares), 16 (open squares) and 17 (filled triangles) of HPr and *P*-HPr during the restrained and unrestrained MD simulations in water. A large change occurs in the φ, ψ torsion angle for His15 upon phosphorylation leading to strain at this position in the *P*-HPr structure. This strain persists during 350 picoseconds of free MD simulation of *P*-HPr, which was performed after the time-averaged restrained MD run. Release of NMR distance restraints during the MD simulations had hardly any effect on the φ, ψ torsion angles in HPr (compare 5 and 6 in Figure 7) and *P*-HPr (compare 7 and 8 in Figure 7), indicating that the local structure is stable during such a free MD simulation. Moreover, in a free MD simulation of *P*-HPr, which started from the same structure of unphosphorylated HPr into which we had introduced the phosphoryl group at His15, the torsion angles of the residues 15, 16 and 17 attained the same values as those found in the restrained MD simulation of *P*-HPr, but only after about 100 picoseconds. Again, this strain remained stable during the remaining 150 picoseconds of the simulation. Nevertheless, we cannot exclude the possibility that the strain at His15 will disappear again after a longer time period than simulated here. The changes in the φ, ψ torsion angles of Thr16 and Arg17 upon phosphorylation are smaller; they are expected to lead to an increase of the $^{3}J_{NHH\alpha}$-coupling constants for Thr16 and Arg17 (Pardi *et al*., 1984), which was verified experimentally (Figure 3). Figure 7 also displays the φ, ψ torsion angles for residues 15, 16 and 17 in the X-ray structures of *B. subtilis*, *S. faecalis* and *E. coli* HPr. The values found for our NMR structure of *E. coli* HPr are close to the ones found in the corresponding X-ray structure. In order to determine whether the strain at residue 16 in *S. faecalis* HPr would be stable in a MD simulation, we used the *S. faecalis* HPr X-ray structure as the starting point of a free MD simulation in water. The strain at residue 16 disappeared soon after the simulation was started (compare 2 with 3 in Figure 7), and average values for the φ, ψ dihedral angles were found, close to those found for all other

Table 3

Structural statistics and atomic r.m.s.d. values

	HPrt	*P*HPrt	*P*HPrf	*Sf*HPr
Violations (nm)†				
Number	25	23	47	
Sum	0.820	0.841	3.703	
Largest	0.073	0.095	0.288	
Average energy (kJ/mol)				
Bonds	97	99	96	83
Angles	354	408	420	345
Impropers	120	141	141	130
Torsion	342	365	364	331
Coulomb	– 5499	– 5532	– 5521	– 5016
Lennard-Jones	– 2634	– 2634	– 2639	– 2661
Atomic r.m.s.d. (nm)‡				
Backbone (N, Ca, CO) res. 2–84	0.080	0.076	0.106	0.102
Backbone (N, Ca, CO) res. 14–19	0.030	0.023	0.033	0.032

All snapshots were energy-minimised in 300 steps of steepest-descent energy minimisation. HPrt and *P*HPrt are the 20 snapshots taken from the 2 time-averaged restrained MD trajectories in water of unphosphorylated and phosphorylated HPr, respectively. *P*HPrf and *Sf*HPr are the 20 snapshots taken from the free MD trajectories in water of *E. coli P*-HPr and *S. faecalis* HPr, respectively.

† The values given are based on $\langle r^{-3}\rangle^{-1/3}$ averages, calculated from the set of HPr configurations, which were compared with the NOE-based distance restraints.

‡ The r.m.s. positional differences are the average values of all pairwise r.m.s.d. values within the set of HPr configurations for the residues given.

unphosphorylated HPrs. Torsion-angle restraints were not applied during these MD simulations.

Determination of the EI binding site

In our earlier work on the determination of the IIA^{mtl} binding site on HPr, we found the most prominent effects of complexation on the five adjacent residues on both sides of the active site His15 and in the loop and helix containing residues 35 to 56 (Van Nuland *et al*., 1993). Figure 8A, B and C plots the $^{15}N/^{1}H$ chemical shift displacement for each amide cross-peak in the ^{15}N HSQC spectrum of the EI/HPr complex at a molar ratio of 1/3.5. Positive and negative shifts up to 0.06 p.p.m. for ^{1}H and up to 0.6 p.p.m. for ^{15}N occur. At a molar ratio of 1/7 the chemical shifts values fall between those of free HPr and of the EI/HPr complex at the molar ratio of 1/3.5. The top section of Figure 8 plots the $^{1}H/^{15}N$ chemical shift vector for each amide cross-peak. It is clear that the binding site for EI on HPr resembles the binding site for the domain IIA on HPr (compare with Figure 8D, which is taken from Van Nuland *et al*., 1993). The two main differences between the binding site for EI and IIA are the effect on Ala20 (no effect by EI, large effect by IIA) and Lys24 (large effect by EI, no effect by IIA). Complexation also leads to measurable changes in chemical shifts of the side-chain amide cross-peaks of Gln51, which disappeared on complexation with IIA^{mtl} (Van Nuland *et al*., 1993). All other side-chain NH_2 groups of the asparagine residues 12 and 38 and glutamine residues 3, 4, 21, 57 and 71, were hardly affected (Shifts <5 Hz) by complexation with EI.

The EI/HPr complex, was diluted with an equal volume of buffer to determine whether dilution would cause the complex to dissociate and the peaks to shift back to their earlier positions. No chemical shift changes in the spectrum occurred after dilution, indicating that binding of EI is complete in the concentration range used here.

Discussion

Structural comparison

Table 6 summarises the structural differences between different HPrs. In general, the X-ray structures of the different unphosphorylated HPrs differ more from the NMR structure of *E. coli P*-HPr than from that of the unphosphorylated form. This is mainly caused by the structural changes that occur at the active site upon phosphorylation, as can be concluded from the increase in the r.m.s. positional differences, calculated only for the active site residues.

The MD simulation starting from the X-ray structure of *S. faecalis* results in some important structural changes. Whereas the overall backbone diverges from all other HPr structures (Table 6), the active centre main-chain positions converge to the common arrangement in the X-ray structures of *B. subtilis* and *E. coli*, and the *E. coli* NMR structure of the unphosphorylated form. Thus the configuration of the active-site peptide residues 14 to 19 is more similar to the rest of the HPr species studied than is the configuration of the entire peptide backbone. We also showed that the strain at residue 16 reported in the X-ray structure was released when the MD simulation was performed, showing φ, ψ torsion angles for the active site residues close to values found for all other HPr structures (see Figure 7). Our data on *P*-HPr on the other hand seem to indicate that strain is introduced upon phosphorylation at

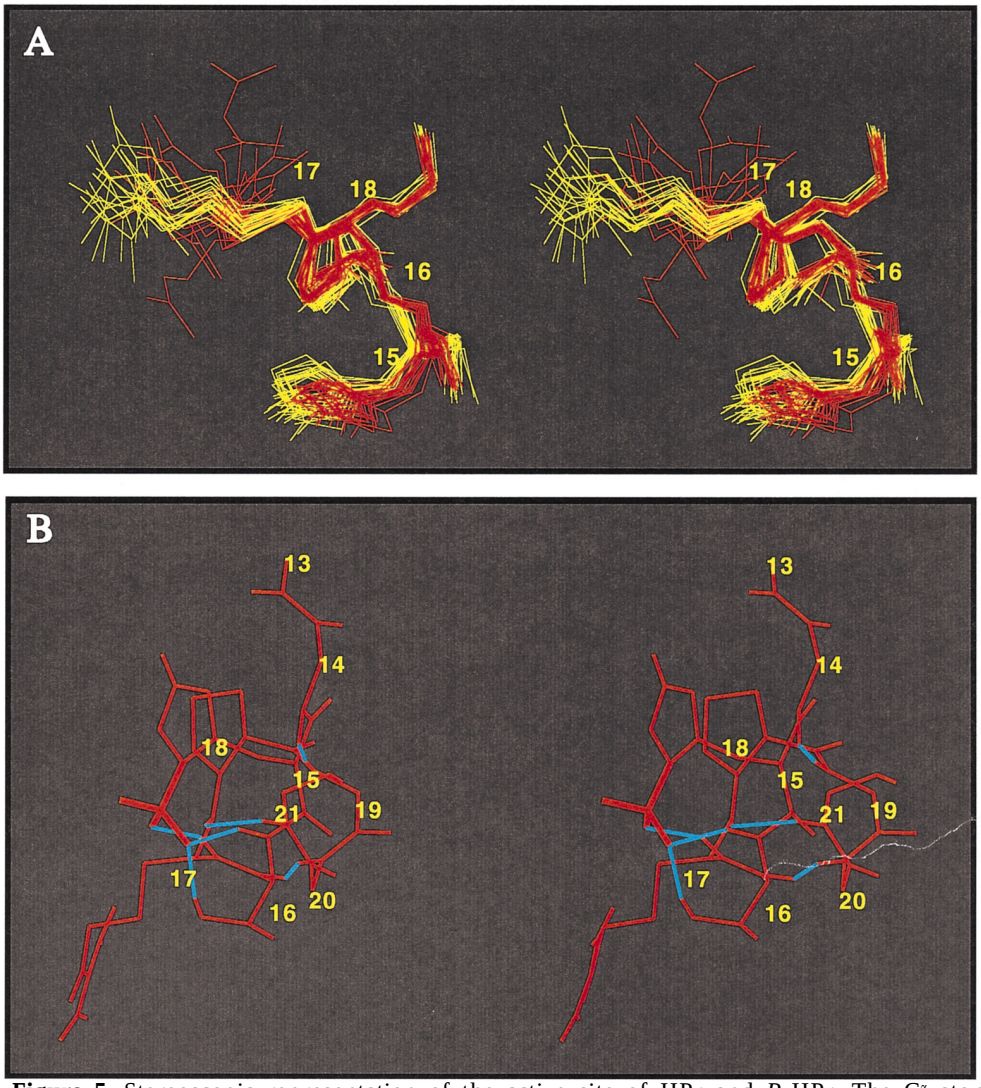

Figure 5. Stereoscopic representation of the active site of HPr and *P*-HPr. The C^{α} atoms are labelled with the corresponding number. A, Two times 20 snapshots taken from the 2 time-averaged restrained MD trajectories of HPr (yellow) and *P*-HPr (red) superimposed such as to optimise the overlay of the backbone atoms of residues 14 to 19 and the side-chain atoms of Pro18. Co-ordinates will be deposited with the Brookhaven Protein Data Bank. B, Hydrogen-bonding network (blue), stabilising the active-site configuration in *P*-HPr. The phosphoryl group is indicated by thick lines.

residue 15. We found no evidence for any such strain at residue 16 in our high-resolution structure of unphosphorylated *E. coli* HPr (Van Nuland *et al*., 1994) and the disappearance of this strain in the MD simulation of the *S. faecalis* HPr structure suggests that it may not be a relevant characteristic of the HPr structure. Consequently, the proposed role of the torsion-angle strain at residue 16 in *S. faecalis* HPr in the phosphorylation / dephosphorylation mechanism (Jia *et al*., 1993*a*, 1994) is not supported by our results. When comparing the X-ray structures of *S. faecalis* HPr with that of *B. subtilis* HPr, which lacked this torsion-angle strain, Jia *et al*. noted that a sulphate ion had cocrystallised in the active site of *B. subtilis* HPr and proposed that the differences between the two X-ray structures reflected a conformational change, which occurred during the phosphorylation / dephosphorylation cycle, assuming that the sulphate could be seen as a phosphate analogue. They suggested that the strain at residue 16 was released upon phosphorylation.

Several groups have suggested that the distance between the His15 ring and the positively charged Arg17 side-chain depends on the protonation state of the imidazole ring. It points away from the guanidino group at low pH in the *S. faecalis* HPr X-ray structure (Jia *et al*., 1994), where the histidine ring is positively charged, while it is in relative close contact in the uncharged state at higher pH in *S. aureus* (Kalbitzer & Hengstenberg, 1993), *B. subtilis* (Herzberg *et al*., 1992) and *E. coli* (Van Nuland *et al*., 1994) HPr. The X-ray structure of *E. coli* HPr was also obtained at low pH (Jia *et al*., 1993*b*), but showed equivalent positions for the His15 and Arg17 side-chains to those found for the structures obtained at physiological pH. The original *S. faecalis* HPr X-ray structure was obtained at pH 5.0 (Jia *et al*., 1993*a*), below its pK_a of 6.1

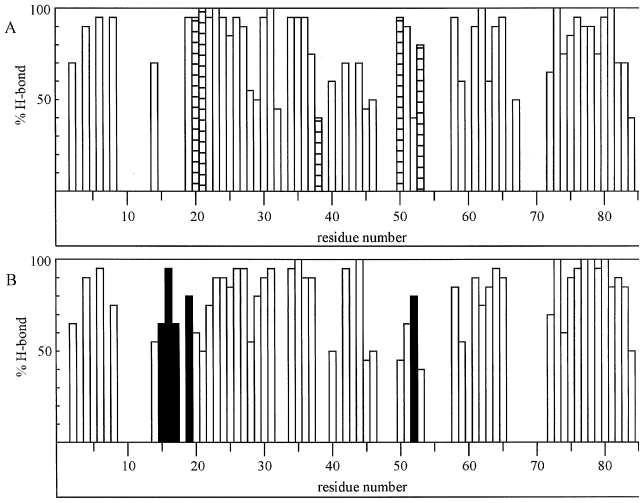

Figure 6. Stability of H-bonds (% H-bond) involving backbone amide protons *versus* the amino acid sequence. The H-bonds that are stable during more than 40% of the time-averaged restrained MD simulations in water of HPr and *P*-HPr are depicted in A and B, respectively. Hatched bars in A correspond to H-bonds that are 30% more stable in HPr than in *P*-HPr. Filled bars in B represent protons that have different H-bond acceptors in the 2 MD simulations.

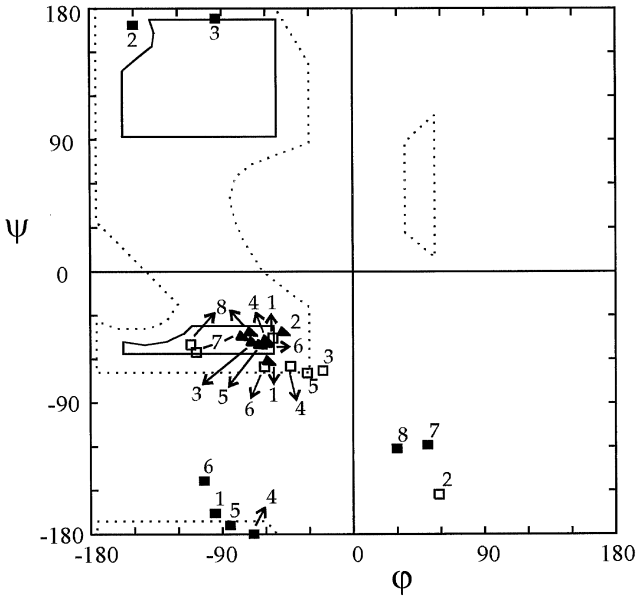

Figure 7. The average φ, ψ torsion angles for residues 15 to 17 (Ramachandran *et al*., 1963), found in the different X-ray structures and values obtained from MD simulations of several forms of HPr. Filled squares correspond to His15; open squares to Thr16 (Ala16 in *S. faecalis* HPr and *B. subtilis* HPr); and filled triangles to Arg17. 1, *B. subtilis* X-ray; 2, *S. faecalis* X-ray; 3, free MD simulation in water of *S. faecalis* HPr; 4, *E. coli* X-ray; 5, time-averaged restrained MD simulation in water of *E. coli* HPr; 6, free MD simulation in water of *E. coli* HPr; 7, time-averaged restrained MD simulation in water of *E. coli P*-HPr; 8, free MD simulation in water of *E. coli P*-HPr.

(Kalbitzer *et al*., 1982). The same authors showed that no structural changes occurred when the crystal was soaked in a solution at pH 7.0 (Jia *et al*., 1994). All of our HPr MD simulations were performed using the charge distribution on the His15 imidazole ring as given in Table 2. This distribution is expected at a pH above the pK_a of His15, which is 5.4 to 5.7 for *E. coli* (Dooijewaard *et al*., 1979; Kalbitzer *et al*., 1982; Anderson *et al*., 1991, 1993). Thus, the simulations were performed with an uncharged imidazole ring, mimicking conditions at physiological pH. Figure 9A shows a stereoscopic representation of the active centre of 20 snapshots taken from the unrestrained MD trajectory of *S. faecalis* HPr. Figure 9B shows the active centre of the X-ray structure of *S. faecalis* HPr together with the X-ray structures of *E. coli* and *B. subtilis* HPr. The positions of the side-chains of residues 15 and 17 do not change much during the simulation on *S. faecalis* HPr with respect to their position in the X-ray structure. This seems to be the main difference between the active site conformation of *S. faecalis* HPr in respect to the other HPrs where the position of the His15 imidazole ring seems to be fixed (see Figure 9B). So, the different positions are independent of the protonation state of the imidazole ring. The Arg17 side-chain occupies different positions in the phosphorylated form of HPr as was shown in Figure 5. This altered position might be essential in the final transfer of the phosphoryl group to A domains of various sugar-specific enzyme IIs.

From NMR data on ^{15}N-histidine-enriched HPr, Van Dijk *et al*. (1990) concluded that both $N^{\epsilon 2}$ protons of His15 and His76 were strongly H-bonded in the unphosphorylated state of HPr. Upon phosphorylation the His15 $H^{\epsilon 2}$ H-bond was lost, while the H-bond involving His76 $H^{\epsilon 2}$ remained stable. A stable H-bond was found for His76 $H^{\epsilon 2}$ to the side-chain $O^{\epsilon 1}$ or $O^{\epsilon 2}$ of Glu25 in the earlier MD simulations on HPr (Van Nuland *et al*., 1994), and in our present MD simulations on HPr and on *P*-HPr, in full agreement with the experimental data. In our earlier MD simulations on HPr using the standard GROMOS (see Van Gunstenen & Berensden, 1987) charges on the histidine ring, we did not observe a stable H-bond to the His15 $H^{\epsilon 2}$. On the basis of the pH sensitivity of the chemical shifts of the Asn12 side-chain NH_2 and the observed NOEs between the imidazole ring and the Asn12 C^{β} protons, we suggested that the best candidate for the H-bond acceptor was the side-chain of Asn12. We also noted that the α-carboxyl group of the C-terminal Glu was sometimes close enough to form a hydrogen bond during the MD simulations in water. In the *E. coli* X-ray structure the His15 $N^{\epsilon 2}$ was found to be ion-paired to the α-carboxyl group of Glu85 (Jia *et al*., 1993*b*). In the present MD simulations on HPr using corrected charges on the histidine ring (Table 2), a stable H-bond is found between the His15 $H^{\epsilon 2}$ and the α-carboxyl group of Glu85 during 80% of the simulation time. This H-bond is not present in the MD simulation on *P*-HPr. Instead, the $H^{\epsilon 2}$ was

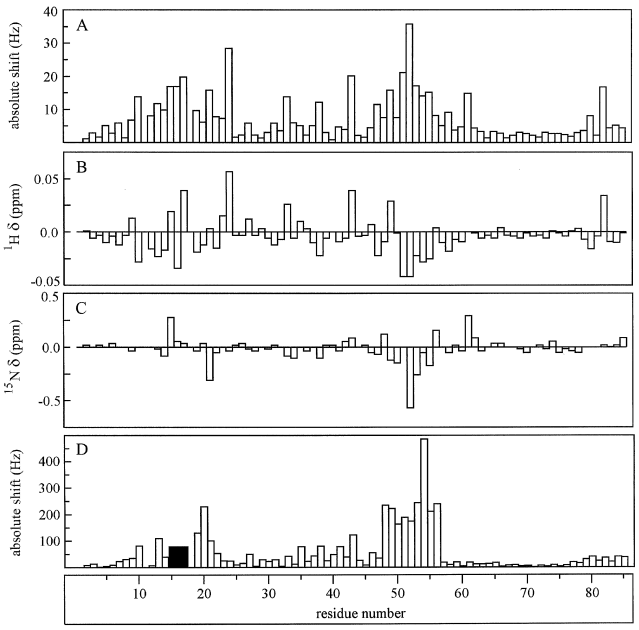

Figure 8. Plots of the change in ^{15}N and ^{1}H chemical shifts (δ) observed for HPr upon adding EI and IIA^{mtl}. A, The absolute shift, defined as the distance over which the ^{15}N-^{1}H cross-peak is displaced in the HSQC spectrum upon adding EI to a molar ratio of 1/3.5 (EI/HPr). B, ^{1}H chemical shift changes. C, ^{15}N chemical shift changes. D, The absolute shift at the end of the titration with IIA^{mtl} (from Van Nuland *et al*., 1993). Filled bars at residues 15, 16 and 17 indicate that the corresponding ^{1}H-^{15}N cross-peak disappeared after addition of IIA^{mtl}.

sometimes close enough to form a H-bond to the Asn12 O$^{\delta 1}$ atom in *P*-HPr.

EI-binding site

Inspection of the residues that experience shifts as a result of complex formation shows that most of them are facing the surface of HPr. In a number of cases they are found on the inner side of helical segments that form contacts with the underlying β-sheet, while other residues in the same segments face outwards and presumably form contacts with EI and/or IIA^{mtl}. Apparently, binding induces structural rearrangements between different elements of the HPr tertiary structure. Figure 8 shows that the binding interface on HPr for EI resembles that for IIA^{mtl}. More charged residues in HPr seem to be involved upon binding to EI, since the ^{1}H-^{15}N frequencies of Gln21, Lys24 and Lys27 are sensitive to binding. It seems that electrostatic interactions are more important in binding EI, while hydrophobic interactions are more important in stabilising the HPr/IIA^{mtl} complex. The same residues on HPr are found to be sensitive to binding the IIA domain of the glucose permease (IIA^{glc}) in *B. subtilis*, as concluded from NMR data (Chen *et al*., 1993) and from modelling studies (Herzberg, 1992). Residues close to the second phosphorylation site Ser46 in *B. subtilis* HPr were also found to be sensitive to the formation of the complex (Chen *et al*., 1993). The Ser46 can only be phosphorylated by an ATP-dependent HPr kinase in Gram-positive bacteria but not in Gram-negative bacteria like *E. coli*. Herzberg (1992) concluded that no major conformational transition is required for the formation of the complex between HPr and IIA^{glc} during the phosphoryl-group transfer. The Arg17 side-chain was found to be ion-paired to two aspartate residues in IIA^{glc}. We showed that the position of the Arg17 side-chain changed upon phosphorylation, which would enable it to make the favourable electrostatic interactions with A domains of various enzyme IIs. However, complete understanding of the mechanism of the phosphoryl-group transfer from EI to HPr and of HPr to the various IIA domains and accompanying structural changes must await the structure determination of the different complexes themselves.

One of the regions that undergo chemical shift

Table 4

The r.m.s. positional differences (nm) between the three X-ray structures and the average structures resulting from the time-dependent restrained MD simulations in water on unphosphorylated and phosphorylated *E. coli* HPr, and the free MD simulation on *S. faecalis* HPr

	B. subt.	*S. faec.*	*Sf*HPr	*E. coli*	HPrt	*P*HPrt
B. subt.	0.0	0.088	0.043	0.041	0.039	0.058
S. faec.	0.073	0.0	0.0604	0.064	0.065	0.083
*Sf*HPr	0.147	0.147	0.0	0.029	0.035	0.059
E. coli	0.166	0.113	0.174	0.0	0.040	0.064
HPrt	0.111	0.114	0.137	0.082	0.0	0.043
*P*HPrt	0.112	0.131	0.153	0.115	0.081	0.0

Values in the upper right part were obtained after superposition on the backbone N, C$^\alpha$ and CO atoms for residues 14 to 19, including the side-chain atoms for residue 18. Values in the lower left part are obtained after superposition on the backbone N, C$^\alpha$ and CO atoms for residues 2 to 84. *B. subt.* is the X-ray *B. subtilis* HPr structure (PDB entry 2HPR), *S. faec.* the X-ray *S. faecalis* HPr structure (PDB entry 1PTF), *Sf*HPr the average from the free MD trajectory in water on *S. faecalis* HPr, *E. coli* the X-ray *E. coli* HPr structure (PDB entry 1POH), HPrt and *P*HPrt the averages from the 2 time-averaged restrained MD trajectories in water on unphosphorylated and phosphorylated HPr, respectively.

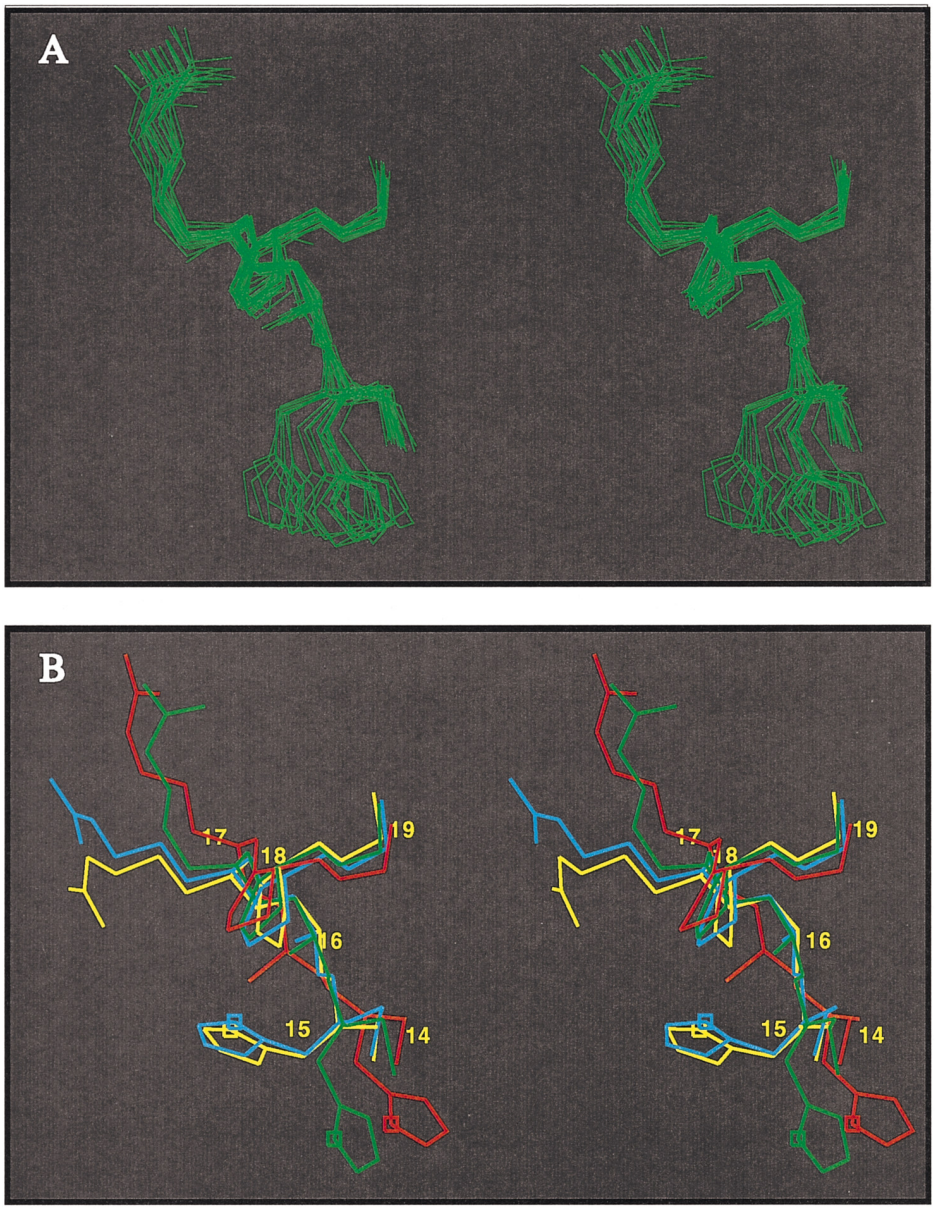

Figure 9. Stereoscopic representation of the active sites of different HPrs. All structures were superimposed such as to optimise the overlay of the backbone atoms of residues 14 to 19 and the side-chain atoms of Pro18. A, Twenty snapshots taken from the unrestrained MD trajectory of *S. faecalis* HPr. B, The 3 X-ray structures and the structure closest to the average structure over the MD simulation of *S. faecalis* HPr (depicted in A). *S. faecalis* (PDB entry 1PTF) in red, *B. subtilis* (PDB entry 2HPR) in yellow, *E. coli* (PDB entry 1POH) in blue, and the structure closest to the average structure over the MD simulation of *S. faecalis* HPr in green. The C^{α} atoms are labelled with the corresponding residue number.

changes upon titration with EI and IIA^{mtl}, as well as upon phosphorylation, is the loop containing the small helix ranging from Leu47 to Thr52. The H-bond network in this helix was destabilised upon phosphorylation (Figure 6). The loop is one of the most poorly defined regions in the NMR structure, indicating possible conformational flexibility, which may be essential for adaptation of this portion of HPr to the binding sites of its various partners.

In this paper we have shown the power of modern NMR spectroscopy. Clearly, NMR is the technique to be used to determine structures of unstable intermediates, like in this case the phosphorylated form of HPr. We also showed that by performing relatively simple NMR experiments on isotope-enriched protein, it is possible to determine the binding interface for various partners of the protein of interest in a very straightforward, fast way, without

Table 5

Composition and concentration of the components used for the EI titration experiment

Sample	[HPr] (mM)	[EI] (mM)	EI/HPr ratio
1	0.85	0.0028	0
2	0.85	0.12	1/7
3	0.43	0.12	1/3.5

knowing the structural details of the various partners.

Materials and Methods

Sample preparation

HPr and P-HPr

The production and purification of uniformly ^{15}N-enriched HPr has been described previously (Van Nuland *et al*., 1992*a*). Enzyme I was purified following published procedures (Robillard *et al*., 1979). A phosphorylation mix (*P*-mix) contained PEP, $MgCl_2$ and DTT in a 50 mM KP_i buffer (pH 7.5). Two NMR samples were prepared, each containing 40 μl ^2H_2O and 500 μl of the *P*–mix added to ^{15}N-enriched Hpr which had been freeze-dried from ^1H_2O. The protein concentration was 5.2 mM. The concentrations of the other components were 90 mM PEP, 0.9 mM DTT and 9 mM $MgCl_2$. NMR spectra were recorded of the unphosphorylated HPr sample. Subsequently, phosphorylation was achieved by adding 50 μl of a 0.2 mM EI solution in 1 mM DTT, 50 mM KP_i buffer (pH 7.5) to the HPr solution and the same spectra were recorded for this *P*-HPr sample.

Determination of the enzyme I binding site of HPr

Three samples were prepared for the titration of ^{15}N-enriched HPr with EI. Table 5 shows the concentrations of the different components. Spectra were recorded for every sample at 20°C. The pH was checked before and after each experiment and was found to be pH 7.50 ± 0.05 in each case.

NMR spectroscopy

All 500 MHz NMR experiments were performed on a Varian Unity 500 NMR spectrometer. The 600 MHz spectra were recorded on a Bruker AM 600 spectrometer at the Bijvoet Centre of the University of Urecht, The Netherlands. All spectra were recorded at 20°C, in a 50 mM potassium phosphate buffer (pH 7.5).

HPr and P-HPr

In one series of experiments we recorded a ^1H-^{15}N high-resolution heteronuclear single-quantum coherence (HSQC) spectrum and a ^1H-^{15}N single-quantum coherence ^1H NOE (^{15}N-HSQC-NOESY) spectroscopy spectrum of unphosphorylated ^{15}N-enriched HPr. Next, after phosphorylation of HPr by the addition of EI, we recorded the same spectra of *P*-HPr. In a similar series of experiments we recorded a ^1H-^{15}N high-resolution heteronuclear multiple-quantum coherence (HMQC) spectrum and a series of 2D NOESY spectra, both of HPr and *P*-HPr. At the end of this latter series, a 2D total correlation (TOCSY) spectrum was recorded on the partially dephosphorylated sample, resulting in a spectrum in which both HPr and *P*-HPr *J*-coupled cross-peaks were detectable. The presence of PEP was checked by recording a 1D ^1H spectrum before and after the build-up series.

The pulse sequence used for the ^{15}N-HSQC-NOESY was described by Majumdar & Zuiderweg (1993); it was adjusted to be used for ^{15}N editing, recorded at 500 MHz. A mixing time of 100 milliseconds was used. Maximum t_1, t_2 and t_3 values were 25.6, 38 and 77 milliseconds, and spectral widths in the $\omega 1$ (^1H), $\omega 2$ (^{15}N) and $\omega 3$ (^1H) domains were 5000, 2000 and 10,000 Hz, respectively. The ^1H carrier was positioned at the water resonance and time-proportional phase incrementation (TPPI) was used to discriminate between positive and negative frequencies in the t_1 evolution period (Bodenhausen *et al*., 1980). Eight t_3 transients were recorded for each t_1,t_2 pair. Total duration of this experiment was about 20 hours.

A series of two-dimensional (2D) NOESY spectra was recorded at 600 MHz, with mixing times of 50, 100 and 150 milliseconds. Maximum t_1 and t_2 values were 63.5 milliseconds and 127.0 milliseconds, respectively, and spectral widths in the $\omega 1$ and $\omega 2$ domains were both 8064.5 Hz. Twentyfour transients were recorded for each t_1,t_2 value. The water resonance was suppressed by presaturation during a 1.5 second relaxation delay. Total duration of this series of experiments was about 18 hours.

The 2D TOCSY spectrum was recorded at 600 MHz using a mixing time of 50 milliseconds MLEV17 mixing sequence (Bax & Davis, 1985). Maximum t_1 and t_2 values were 63.5 milliseconds and 127.0 milliseconds, respectively, and spectral widths in the $\omega 1$ and $\omega 2$ domains were both 8064.5 Hz. Sixteen transients were recorded for each t_1,t_2 value. A relaxation time of one second was used. Total duration of this experiment was about three hours.

$^3J_{NHH\alpha}$ couplings were obtained from a 2D ^1H-^{15}N high-resolution HMQC spectrum (Kay & Bax, 1990) at 600 MHz. Maximum t_1 and t_2 values were 384 milliseconds and 63.5 millieconds, respectively, and spectral widths in the $\omega 1$ (^{15}N) and $\omega 2$ (^1H) domains were 2000 Hz and 8064.5 Hz. Total duration of this experiment was 30 minutes. The data were zero filled in the $\omega 1$ domain to give a final digital resolution of 1.03 Hz / point.

Enzyme I binding site

The EI binding site on HPr was determined by recording heteronuclear ^1H-^{15}N-HSQC spectra at 500 MHz in the presence of varying concentrations of EI. Maximum t_1 and t_2 values were 64 milliseconds and 77 milliseconds, respectively, and spectral widths in the $\omega 1$ (^{15}N) and $\omega 2$ (^1H) domains were 2000 Hz and 6666 Hz. The ^1H carrier was positioned at the water resonance and, during the acquisition period, ^{15}N decoupling was achieved by a broad-band Waltz decoupling sequence using a radio frequency field of $\gamma B_1 = 1$ kHz. Water was suppressed by two orthogonal spin-lock pulses, of two and six milliseconds, applied during the reverse-INEPT part of the pulse sequence (Messerle *et al*., 1989).

Table 6

Dipole preserving charges (Thole & Van Duijnen, 1983) and GROMOS charge distribution on the imidazole ring of His15 in the unphosphorylated (net charge 0) and phosphorylated (net charge, − 1) form

	Imidazole		P-imidazole	
Atom	Charge	GROMOS†	Charge	GROMOS
C^{γ}	+ 0.22	+ 0.10 (+ 0.13)	+ 0.40	+ 0.20
$C^{\delta 2}$	+ 0.15	+ 0.10 (0)	+ 0.05	0
$N^{\epsilon 2}$	− 0.60	− 0.35 (0)	− 0.68	− 0.40
$H^{\epsilon 2}$	+ 0.45	+ 0.30 (+ 0.19)	+ 0.46	+ 0.30
$C^{\epsilon 1}$	+ 0.33	+ 0.30 (+ 0.26)	+ 0.41	+ 0.40
$N^{\delta 1}$	− 0.56	− 0.45 (− 0.58)	− 0.58	− 0.50
$N^{\delta 1}P$			+ 2.15	+ 0.95
O1P			− 1.11	− 0.65
O2P			− 1.11	− 0.65
O3P			− 1.11	− 0.65

† Standard GROMOS charges are given in parenthesis.

Structure calculations

General

All MD simulations described here were done in water at 300 K, using the GROMOS 37C4 force field parameter set in a truncated octahedron box containing 2921 water molecules in the case of *E. coli* HPr and *P*-HPr (Van Gunsteren & Berendsen, 1987). Details concerning the different parameters used are described in our previous work on unphosphorylated HPr (Van Nuland *et al*., 1994).

Strategy

One of the structures resulting from the time-averaged restrained MD simulations of HPr, described earlier (Van Nuland *et al*., 1994), was used to introduce the phosphate at the $N^{\delta 1}$ of His15 using the Polygen molecular graphics software package QUANTA. The charge distribution for the unphosphorylated and phosphorylated imidazole ring were calculated *ab initio* and converted into appropriate GROMOS charges (see Table 6). The phosphate group was handled as a separate charge group. This structure was then energy-minimised using 100 steps of steepest-descent energy minimisation, followed by a MD simulation in water. During the first ten picoseconds of the 20 picosecond equilibration period, the protein molecule was position restrained using a force constant of 8000 kJ mol^{-1} nm^{-2}, decreasing every two picoseconds by 2000 kJ mol^{-1} nm^{-2}. At the same time intervals, distance restraining was applied by increasing the force constant from 0 to 1000 kJ mol^{-1} nm^{-2}. The simulation was continued for another ten picosecond equilibration, followed by 50 picoseconds of restrained MD and subsequently by 200 picoseconds of time-averaged restrained MD (Torda *et al*., 1990), following the procedure in Van Nuland *et al*. (1994). For a comparable treatment of unphosphorylated HPr, the same time-averaged restrained MD simulation was carried out on the unphosphorylated HPr structure used above. The simulation was also continued in the way described for *P*-HPr, excluding the first ten picoseconds of equilibration. Snapshots were taken every ten picoseconds from the time-averaged restrained MD simulation of unphosphorylated and phosphorylated HPr in water, and will be referred to as the HPrt and *P*HPrt MD-clusters, respectively. Both time-averaged restrained MD simulations of HPr and *P*-HPr were continued for another 200 picoseconds without any distance restraining, and will be referred to as the HPrf and *P*HPrf MD clusters, respectively.

The *S. faecalis* HPr X-ray structure (PDB accession number 1PTF) was also used to start a free MD simulation in a truncated octahedron box containing 3483 water molecules, including the 100 crystal water molecules. First, Ala83 was replaced by lysine, as in the wild-type protein, and a C-terminal glutamate was added using QUANTA. This structure was then energy-minimised with 100 steps of steepest-descent energy minimisation, followed by a molecular dynamics simulation in water. After a 30 picosecond equilibration period as described above, but now without distance restraining, the simulation was continued for 200 picoseconds without any restraining. Snapshots were taken every ten picoseconds, and will be referred to as the *Sf*HPr MD cluster.

Acknowledgements

This research was supported by the Netherlands Foundation for Chemical Research (SON) with financial aid from the Netherlands Organisation for Scientific Research (NWO).

The SNARF program, written by Frans van Hoesel, was used for processing, visualising and analysing all NMR data sets. We thank Varian for providing us with the triple-resonance probe. We thank Ria ten Hoeve-Duurkens for the purification of enzyme I. We thank Rob Kaptein for providing instrument time on the Bruker 600 MHz spectrometer in Utrecht. We thank Joachim Grötzinger, Alex de Vries and Herman Berendsen for creating the phospho-histidine building block.

References

Anderson, J. W., Bhanot, P., Georges, F., Klevit, R. E. & Waygood, E. B. (1991). Involvement of the carboxy-terminal residue in the active site of the histidine-containing protein, HPr, of the phospho-enolpyruvate:sugar phosphotransferase system. *Biochemistry*, **30**, 9601–9607.

Anderson, J. W., Pullen, K., Georges, F., Klevit, R. E. & Waygood, E. B. (1993). The involvement of the arginine-17 residue in the active site of the histidine-containing protein, HPr, of the phospho-enolpyruvate:sugar phosphotransferase system of *Escherichia coli*. *J. Biol. Chem.* **268**, 12325–12333.

Bax, A. & Davis, D. G. (1985). MLEV-17 based two-dimensional homonuclear magnetisation transfer spectroscopy. *J. Magn. Reson.* **65**, 355–360.

Bodenhausen, G., Vold, R. L. & Vold, R. R. (1980). Multiple quantum spin-echo spectroscopy. *J. Magn. Reson.* **37**, 93–106.

Chen, Y., Reizer, J., Saier, M. H., Jr, Fairbrother, W. J. & Wright, P. E. (1993). Mapping the binding interfaces of the proteins of the bacterial phosphotransferase system, HPr and IIA^{glc}. *Biochemistry*, **32**, 32–37.

Dooijewaard, G., Roossien, F. F. & Robillard, G. T. (1979). *Escherichia coli* phosphoenol-pyruvate:sugar phosphotransferase system. Copurification of HPr and 1-6 Glucan. *Biochemistry*, **18**, 2990–2996.

Hammen, P. K., Waygood, E. B. & Klevit, R. E. (1991). Reexamination of the secondary and tertiary structure of histidine-containing protein of *Escherichia coli* by homonuclear and heteronuclear NMR spectroscopy. *Biochemistry*, **30**, 11842–11850.

Herzberg, O. (1992). An atomic model for protein-protein phosphoryl group transfer. *J. Biol. Chem.* **267**, 24819–24823.

Herzberg, O., Reddy, P., Sutrina, S., Saier, M. H., Reizer, J. & Kapafia, G. (1992). Structure of the histidine-containing phosphocarrier protein HPr from *Bacillus subtilis* at 2.0 Å resolution. *Proc. Nat. Acad. Sci., U.S.A.* **89**, 2499–2503.

Hol, W. G. J., Van Duijnen, P. Th. & Berendsen, H. J. C. (1978). The α-helix dipole and the properties of proteins. *Nature (London)*, **273**, 443–446.

Jia, Z., Vandonselaar, M., Quail, J. W. & Delbaere, L. T. J. (1993*a*). Active-centre torsion-angle strain revealed in 1.6 Å-resolution structure of histidine-containing phosphocarrier protein. *Nature (London)*, **361**, 94–97.

Jia, Z., Quail, J. W., Waygood, E. B. & Delbaere, L. T. J. (1993*b*). The 2.0-Å resolution structure of *Escherichia coli* histidine-containing phosphocarrier protein HPr. *J. Biol. Chem.* **268**, 22490–22501.

Jia, Z., Vandonselaar, M., Hengstenberg, W., Quail, J. W. & Delbaere, L. T. J. (1994). The 1.6-Å structure of histidine-containing phosphotransfer protein HPr from *Streptococcus faecalis*. *J. Mol. Biol.* **236**, 1341–1355.

Johnson, L. N. & Barford, D. (1993). The effects of phosphorylation on the structure and function of proteins. *Annu. Rev. Biophys. Biomol. Struct.* **22**, 199–232.

Kalbitzer, H. R. & Hengstenberg, W. (1993). The solution structure of the histidine-containing protein (HPr) from *Staphylococcus aureus* as determined by two-dimensional ^{1}H-NMR spectroscopy. *Eur. J. Biochem.* **216**, 205–214.

Kalbitzer, H. R., Hengstenberg, W., Rösch, P., Muss, P., Bernsmann, P., Engelmann, R., Dörschung, M. & Deutcher, J. (1982). HPr proteins of different micro-organisms studied by hydrogen-1 high resolution of nuclear magnetic resonance: similarities of structures and mechanisms. *Biochemistry*, **21**, 2879–2885.

Kay, L. E. & Bax, A. (1990). New methods for the measurement of NH-CαH coupling constants in ^{15}N-labelled proteins. *J. Magn. Reson.* **86**, 110–126.

Live, D. H., Davis, D. G., Agosta, W. C. & Cowburn, D. (1984). Long range hydrogen bond mediated effects in peptides: ^{15}N NMR study of Gramicidin S in water and organic solvents. *J. Amer. Chem. Soc.* **106**, 1939–1941.

Lolkema, J. S. & Robillard, G. T. (1993). The enzyme II of the phosphoenolpyruvate-dependent carbohydrate transport systems. In *The New Comprehensive Biochemistry: Pumps, Carriers and Channels* (de Pont, J. J. H. H. M., ed.), pp. 135–167, Elsevier/North Biomedical Press, Amsterdam.

Majumdar, A. & Zuiderweg, E. R. P. (1993). Improved ^{13}C-resolved HSQC-NOESY spectra in H_2O, using pulsed field gradients. *J. Magn. Reson.* **102**, 242–244.

Messerle, B. A., Wider, G., Otting, G., Weber, C. & Wüthrich, K. (1989). Solvent suppression using a spin lock in 2D and 3D NMR spectroscopy with H_2O solutions. *J. Magn. Reson.* **85**, 608–613.

Pardi, A., Billeter, M. & Wütrich, K. (1984). Calibration of the angular dependence of the amide proton-C$^{\alpha}$ proton coupling constants, $^{3}J_{\mathrm{HN}\alpha}$, in a globular protein. *J. Mol. Biol.* **180**, 741–751.

Postma, P. W., Lengeler, J. W. & Jacobson, G. R. (1993). Phosphoenolpyruvate: carbohydrate phosphotransferase system of bacteria. *Microbiol. Rev.* **57**, 543–594.

Ramachandran, G. N., Ramakrishnan, C. & Sasisekharan, V. (1963). Stereochemistry of polypeptide chain configurations. *J. Mol. Biol.* **7**, 95–99.

Reizer, J., Hoischen, C., Reizer, A., Pham, T. N. & Saier, M. H. (1993). Sequence analyses and evolutionary relationships among the energy-coupling proteins Enzyme I and HPr of the bacterial phosphoenolpyruvate:sugar phosphotransferase system. *Protein Sci.* **2**, 506–521.

Robillard, G. T., Dooijewaard, G. & Lolkema, J. (1979). *Escherichia coli* phosphoenolpyruvate dependent phosphotransferase system: complete purification of Enzyme I by hydrophobic interaction chromatography. *Biochemistry*, **18**, 2984–2989.

Thole, B. T. & Van Duijnen, P. Th. (1983). A general population analysis preserving the dipole moment. *Theor. Chim. Acta*, **63**, 209–221.

Torda, A. E., Scheek, R. M. & Van Gunsteren, W. F. (1990). Time-averaged nuclear Overhauser effect distance restraints applied to Tendamistat. *J. Mol. Biol.* **214**, 223–235.

Van Dijk, A. A., de Lange, L. C. M., Bachovchin, W. W. & Robillard, G. T. (1990). Effect of phosphorylation on hydrogen-bonding interactions of the active site histidine of the phosphoenolpyruvate-dependent phosphotransferase system determined by ^{15}N NMR spectroscopy. *Biochemistry*, **29**, 8164–8171.

Van Gunsteren, W. F. & Berendsen, H. J. C. (1987). *GROningen MOlecular Simulation (GROMOS) library manual*, Biomos, Groningen, The Netherlands.

Van Nuland, N. A. J., van Dijk, A. A., Dijkstra, K., van Hoesel, F. H. J., Scheek, R. M. & Robillard, G. T. (1992*a*). Three-dimensional ^{15}N-^{1}H-^{1}H and ^{15}N-^{13}C-^{1}H nuclear magnetic resonance studies of HPr, a central component of the phosphoenol-pyruvate dependent phosphotransferase system of *Escherichia coli*. *Eur. J. Biochem.* **203**, 483–491.

Van Nuland, N. A. J., Grötzinger, J., Dijkstra, K., Scheek, R. M. & Robillard, G. T. (1992*b*). Determination of the three-dimensional solution structure of the histidine-containing phosphocarrier protein HPr from *Escherichia coli* using multidimensional NMR spectroscopy. *Eur. J. Biochem.* **210**, 881–891.

Van Nuland, N. A. J., Kroon, G. J. A., Dijkstra, K., Wolters, G. K., Scheek, R. M. & Robillard, G. T. (1993). The determination of the IIAmtl binding site on HPr of the *Escherichia coli* phosphoenol-pyruvate dependent phosphotransferase system. *FEBS Letters*, **315**, 11–15.

Van Nuland, N. A. J., Hangyi, I. W., Van Schaik, R. C., Berendsen, H. J. C., Van Gunsteren, W. F., Scheek, R. M. & Robillard, G. T. (1994). The high-resolution structure of the histidine-containing phosphocarrier protein HPr from *Escherichia coli* determined by restrained molecular dynamics from nuclear magnetic resonance nuclear Overhauser effect data. *J. Mol. Biol.* **237**, 544–559.

Waygood, B. E., Erickson, E., El-Kabbani, O. A. L. & Delbaere, L. T. J. (1985). Characterisation of phosphorylated histidine-containing protein (HPr) of the bacterial phosphoenolpyruvate:sugar phosphotransferase system. *Biochemistry*, **24**, 6938–6945.

Weigel, N., Powers, D. A. & Roseman, S. (1982). Sugar transport by the bacterial phosphotransferase system. *J. Biol. Chem.* **257**, 14499–14509.

Edited by P. E. Wright

(Received 29 August 1994; accepted 20 October 1994)